Research Article

Lixia Guo, Tianyu Liang, and Ling Zhong*

Early age temperature effect of cemented sand and gravel based on random aggregate model

https://doi.org/10.1515/secm-2025-0059
received April 15, 2025; accepted May 30, 2025

Abstract: This study investigates the risk of early-age cracking in cemented sand gravel by modeling it as a two-phase material (aggregate and mortar) from a mesoscopic perspective. A mathematical model incorporating mesoscopic components was developed to simulate the temperature stress field under different heat dissipation conditions. Key findings include: (1) Early-age heat release occurs primarily in the mortar, leading to uneven temperature distribution (low in aggregate, high in mortar), which becomes uniform as hydration ends. Stress concentration is observed at aggregate–mortar interfaces. (2) Mesoscopic component consideration reveals local stress concentration, unlike models ignoring meso-components. (3) External heat dissipation conditions significantly affect temperature effects. Under adiabatic conditions, larger deformations occur at mortar–aggregate intersections and increase over time. In heat dissipation states, deformation is higher at boundaries, unevenly distributed, and decreases over time. This research highlights the importance of mesoscopic considerations in understanding and mitigating early-age cracking risks in cemented sand gravel.

Keywords: cemented gravel, thermodynamic properties, stochastic aggregate modeling, temperature response, finite element calculation

*** Corresponding author: Ling Zhong,** School of Water Conservancy, North China University of Water Resources and Electric Power, Zhengzhou, 450046, China; Henan Key Laboratory of Water Environment Simulation and Treatment, Zhengzhou, 450002, China, e-mail: zhongling@ncwu.edu.cn
Lixia Guo: School of Water Conservancy, North China University of Water Resources and Electric Power, Zhengzhou, 450046, China; Henan Key Laboratory of Water Environment Simulation and Treatment, Zhengzhou, 450002, China, e-mail: guolx@126.com
Tianyu Liang: School of Water Conservancy, North China University of Water Resources and Electric Power, Zhengzhou, 450046, China, e-mail: 941735134@qq.com

1 Introduction

Cemented sand and gravel (CSG) [1–5] uses less cementitious materials, unscreened aggregates, and small hydration reaction compared to ordinary concrete, so the on-site temperature control measures are not as strict as those for concrete dams. However, its ability to resist deformation is poor. With the progress of hydration reaction, more and more heat is accumulated inside the structure, resulting in an internal thermal expansion effect. Under the constraint of boundary conditions, temperature stress is formed. It is precisely because of the heterogeneity, nonlinearity, and anisotropy of CSG. Therefore, the temperature gradient is different everywhere in the structure, and the temperature stress is also different. The dam body produces temperature cracks on the surface or inside, which will reduce its durability. Therefore, it is important to explore the development law of temperature stress inside the structure, so that it is within the controllable range, to prevent the generation and development of temperature cracks [6,7] in the early-age cemented gravel dam structure, and to prolong the service life of the dam structure.

There are few existing studies on temperature stress and temperature control of cemented gravel dams, Wu *et al.* [8], combined with Shoukoubu cemented gravel dam test data, numerically simulated the temperature stress change rule of the dam body under different working conditions. Liu *et al.* [9] analyzed the temperature stress field of the Shoukoubu cemented gravel dam. Liu [10] studied the temperature stress field of a rubberized gravel dam. Wu *et al.* [11] used a three-dimensional finite-element simulation method to analyze the temperature stress of a 100-m dam. Xu [12] investigated the effects of factors such as air temperature, dam height, and pouring interval on the temperature stress of cemented gravel dams. Fu [13] performed a numerical simulation of the temperature stress field for the Shoukoubao cemented gravel dam and found that there was a significant temperature effect on the dam during the construction period. Zhao and He [14] proposed a temperature field calculation method applicable to cemented gravel materials by considering the thermal–mechanical properties and seepage

characteristics of cemented gravel materials. Cai *et al.* [15] investigated the creep temperature stresses of different adhesive columns. Chen and Zheng [16] studied the structural damage of cemented gravel materials under the conditions of freezing and thawing based on the freeze and thawing damage law. Jiang *et al.* [17] conducted an adiabatic temperature rise test. Numerical simulation is essential for capturing the mesoscale thermal–mechanical behavior of CSG, as demonstrated by advanced approaches like CT-image-driven modeling [18,19], which validate the critical role of a mesostructure in heterogeneous material analysis.

In this article, the temperature effect of early-age CSG is studied. From a mesoscopic perspective, it is regarded as a two-phase material of aggregate and mortar. A random aggregate model is constructed, and the mesoscopic parameters are inverted through laboratory tests. The temperature stress field under different heat dissipation conditions considering and not considering the mesoscopic components is compared and analyzed. It is found that the heat release of early-age mortar leads to the temperature difference between aggregate and mortar, and the interface is prone to stress concentration, and the mesoscopic model will show local stress concentration. Different heat dissipation conditions will make the temperature stress distribution and deformation law different. The research provides a theoretical basis for the early crack control of CSG dams.

2 Numerical simulation methods

2.1 Stochastic aggregate modeling for cemented gravels

CSG is made of naturally graded sand and gravel material or excavated abandoned riverbed sand and gravel material. In principle, it is not screened. According to Feng *et al.* [20], the study shows that the sand layer and gravel layer are alternately distributed, and the grading distribution is uneven. Figure 1 shows the 12 groups of sand and gravel material gradation and fuller gradation curve in the project site.

Based on the aggregate characteristics of CSG, three-dimensional aggregate is randomly generated to determine the distribution of aggregate according to the three-dimensional grading curve of CSG in the field. The plane is randomly intercepted in the three-dimensional model, and the total area of aggregate in each particle size interval is calculated on the plane, so as to obtain the cumulative distribution function of the two-dimensional aggregate mass

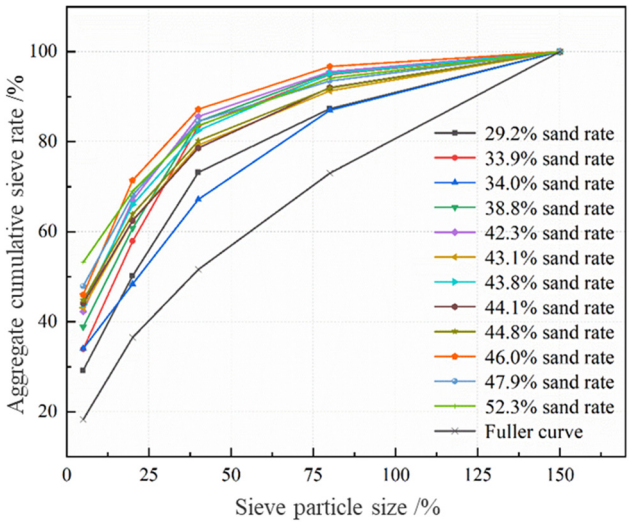

Figure 1: Gravel gradation and Fuller gradation curve.

and ultimately generate the number of two-dimensional aggregate particles to meet the specific grading. The specific process is shown in Figure 2.

The number of aggregates in each particle size interval was then calculated by

$$A_{\mathrm{gg}}[D_s, D_{s+1}] = \frac{P_{2\mathrm{A}}(D_{s+1}) - P_{2\mathrm{A}}(D_s)}{P_{2\mathrm{A}}(D_{\max}) - P_{2\mathrm{A}}(D_{\min})} \times R_{\mathrm{agg}} \times A_{\mathrm{con}}, \quad (2.1)$$

where A_{gg} is the aggregate area of particle size in $[D_s, D_{s+1}]$; $P_{2\mathrm{A}}$ is the aggregate accumulation distribution function for a certain particle size; R_{agg} is the area ratio of coarse aggregate, generally taken as 0.35–0.45; and A_{con} is the area of cemented gravel.

The morphology and distribution of the coarse aggregate of the cemented gravel specimen have randomness, and random variables are needed in the finite-element analysis. The Monte Carlo method is used to set up the random variables for the coarse aggregate placement. The common forms of distribution of the random variables are uniform, logarithmic, and normal, *etc.*, among which the most basic form of distribution is the uniform distribution, which assumes that there is a set of uniform, independent random variables distributed in the interval [0, 1]. The probability density function of X can be expressed as

$$f(x) = \begin{cases} 1 & x \in [0,\ 1] \\ 0 & x \notin [0,\ 1] \end{cases}. \quad (2.2)$$

A subsample sequence $[X_n]$ is generated by randomly drawing from the random variable X. In this article, by generating the aggregate random circle and the bond belt boundary random circle, dividing the quadrants within the inner and outer circles, determining the number of corner points in

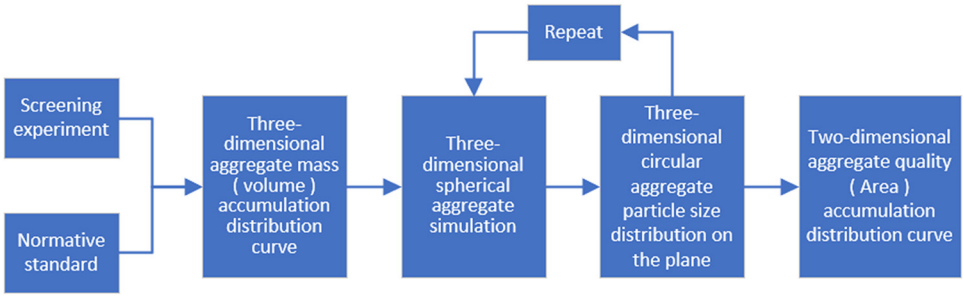

Figure 2: Method for determining the mass cumulative distribution function of two-dimensional aggregates of any gradation.

Table 1: Adiabatic temperature rise test results

Mold temperature (°C)	Appreciation						
	0.5 day (°C)	1 day (°C)	2 day (°C)	3 day (°C)	4 day (°C)	7 day (°C)	Supreme (°C)
32.25	5.59	9.78	13.8	15.7	15.22	15.01	15.23

each quadrant, generating the coordinates of the corner points, and finally connecting the corner points to generate the polygon [21,22].

2.2 Inverse analysis of fine-scale parameters

Because the fine material parameters are difficult to measure directly by indoor tests, these parameters are obtained by inverting the indoor adiabatic temperature rise test. The test uses a Φ400 × 400 mm three-dimensional cylinder of CSG, and the aggregate is a secondary distribution. In this article, the design of the mix ratio of the adiabatic temperature rise test of CSG is based on the mix ratio of the CSG dam of the Shanxi Shoukoubao Reservoir. The water–binder ratio of the adiabatic temperature rise test is 1.58, the sand ratio is 0.418, the cement is 50 kg/m^3, the fly ash is 40 kg/m^3, the coarse aggregate is 1,233 kg/m^3, and the medium coarse sand is 885 kg/m^3 records the temperature change curve after pouring. On this basis, numerical simulation of the above test was carried out, and its fine view parameters were obtained

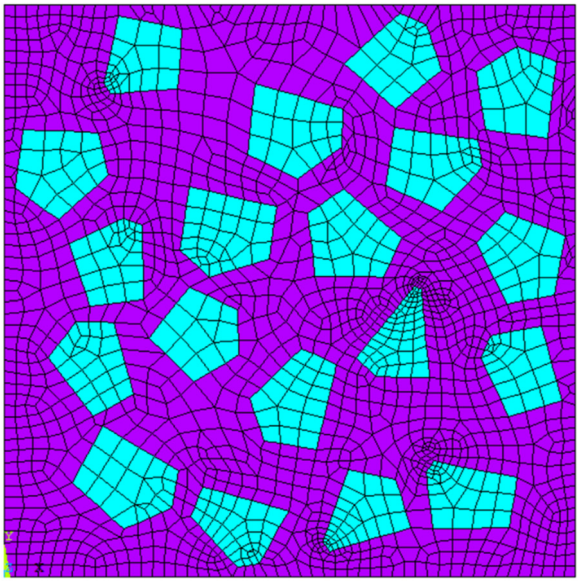

Figure 3: Random polygonal aggregate model of cementitious sand gravel.

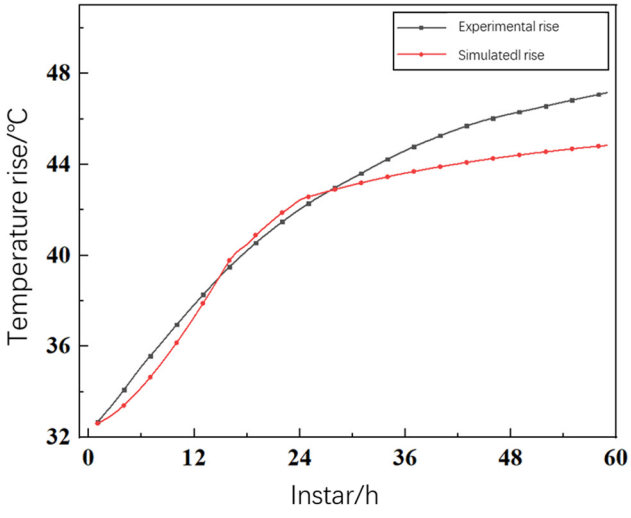

Figure 4: Comparison of temperature change curves.

Table 2: Table of thermal parameters

Individual parts making up a compound	Thermal conductivity [kJ/(m h °C)]	Thermal conductivity [kJ/(m h °C)]	Specific heat capacity [kJ/ (kg °C)]
Mortar (building)	2.06	15.00	0.00
Aggregate	9.90	0.20	0.00

by inversion. Because of more thermal parameters, this article mainly focuses on the inversion of sensitive adiabatic temperature rise and thermal conductivity coefficient, in which the model of adiabatic temperature rise adopts the composite exponential model [23–25].

The adiabatic temperature rise test uses a BY-ATC/B-type concrete thermophysical parameter tester to track and measure the temperature change of the cemented gravel specimen for 7 day, and the test results are shown in Table 1.

From the results, it can be seen that with the hydration reaction, the temperature rises gradually and stabilizes after 3 day and reaches the maximum adiabatic temperature rise at about 4 day, which is 15.23°C; the maximum adiabatic temperature rise rate occurs at about 6 h, and the maximum adiabatic temperature rise rate value is about 0.35 (°C/h).

In order to solve the problems of a cumbersome traditional inversion process and unclear modeling of a mathematical relationship between parameters of CSG, the inversion of fine parameters was carried out according to the response surface method of the previous group [26]. A two-dimensional random aggregate model of Φ400 × 400 mm is established as shown in Figure 3.

The adiabatic temperature rise test data are brought into the response surface model as the inversion target, requiring more than 97% guarantee rate, and the basic parameters are brought into the response surface software to solve the temperature field regression equation. The inversion results are shown in Table 2.

The adiabatic temperature rise for the macroscopic cemented gravel specimen is $15.23\text{-}(1\text{-}\exp(-0.0208\text{-}\tau^{1.2356}))$°C and for the mortar is $32.55\text{-}(1\text{-}\exp(-0.0208\text{-}\tau^{1.2356}))$°C.

The inversion fine view parameters were brought into the finite-element model for solving to obtain its temperature ephemeral curve and compared with the indoor test results as shown in Figure 4.

The similar temperature rise trends and close agreement between simulation and experimental results indicate that the numerical analysis of the temperature field for cemented sand and gravel is highly reliable.

To further calculate the thermal stress response, the following fine-scale mechanical parameters shown in

Table 3: Parameter description

Sports event	Coarse aggregate	Mortar (building)	Cohesive sandstone
Coefficient of linear expansion (1/°C)	8.45	15.00	8.49
Poisson's ratio	0.16	0.20	0.16

Table 4: Calculate the working conditions and their boundary conditions

Condition no.	Stress field boundary conditions	Temperature field boundary conditions	Note
1	Bottom full constraint	Insulation all around	Model validation, comparison with indoor adiabatic temperature rise test results
2		Peripheral heat dissipation	Comparison of working conditions 1
3		Two sides insulated, two sides heat dissipation	Consideration of fine-grained components
4		Two sides insulated, two sides heat dissipation	Comparison of Case 3 without consideration of fine-grained components

Table 3 were used with reference to the relevant literature [27,28].

3 Thermal stress analysis of cemented gravel considering fine-scale components

3.1 Computational conditions and boundary conditions

In order to explore the distribution and trend of temperature and stress field inside the cemented gravel specimen, the following four working conditions are set as shown in Table 4. Under different working conditions, there are differences in the internal temperature stress field of CSG specimens. In order to explore the distribution and change trend of the internal temperature stress field of CSG specimens and to accurately describe the law, numerical simulation studies were carried out under four working conditions. Among them, working conditions 1 and 2 were compared, working conditions 3 and 4 were compared, working conditions 1, 2, and 3, the microscopic components—such as the distinct phases of mortar and aggregate—were included in the simulation. Only the mortar was assumed to release heat, while the aggregate did not. In contrast, working condition 4 did not consider microscopic components; the specimen was treated as a homogeneous material, and all elements were assumed to release heat uniformly.

The temperature field is calculated with an initial pouring temperature of 32.25°C. Case 1 is a verification of the adiabatic temperature rise test, with adiabatic heat all around; Case 2 is a state of full heat dissipation all around, with the third type of boundary conditions; and Cases 3 and 4 are the states of adiabatic heat on the left side and the bottom and heat dissipation on the right side and on the top, with the heat dissipation surface exchanging heat with the external medium. The external ambient temperature is 25°C.

The stress field is analyzed with the model fully constrained at the bottom, and the other faces are free.

The selection of temporal sampling points for temperature field visualization was carefully optimized according to the distinct thermal evolution characteristics of each working condition. For the adiabatic case (Case 1), six representative time points were systematically selected to comprehensively capture the complete thermal transition process, given its relatively gradual temperature variation. In contrast, for the heat dissipation cases (Cases 2–4), the analysis focused on key temporal nodes that most effectively characterize the thermal behavior.

3.2 Analysis of temperature field results

3.2.1 Case 1 (adiabatic temperature rise test verification case)

The simulated specimen tends to an isothermal state.

3.2.2 Working condition 2

From Figure 6, comparing the trend of temperature field distribution of Cases 1 and 2 at the same moment, it can be found that the temperature is higher at the same moment in Case 1, the temperature difference is smaller, and the distribution of high-temperature region is different, which is due to adiabatic condition 1, the heat released by the high-temperature mortar is transferred to the low-temperature aggregate, and eventually the internal temperature of the specimen is getting higher and higher, and is maintained at a certain value, while Case 2 is in the state of full dissipation of heat, and heat is exchanged at the boundary, and the temperature is changing more quickly. As time proceeds, the internal temperature of the specimen tends to approach the ambient temperature.

3.2.3 Working condition 3

On the adiabatic surface, the heat released by mortar accumulates and causes a temperature rise, whereas on the heat dissipation surface, although the mortar also releases heat, it is quickly lost to the environment. As hydration progresses and the amount of reactive cementitious material decreases, the temperature distribution gradually becomes more uniform and the temperature difference diminishes.

3.2.4 Working condition 4

The comparison of conditions 3 and 4 in Figure 8 shows that the temperature distributions of the two models are not exactly the same, the temperature distribution of the fine model is more drastic, and the temperature difference

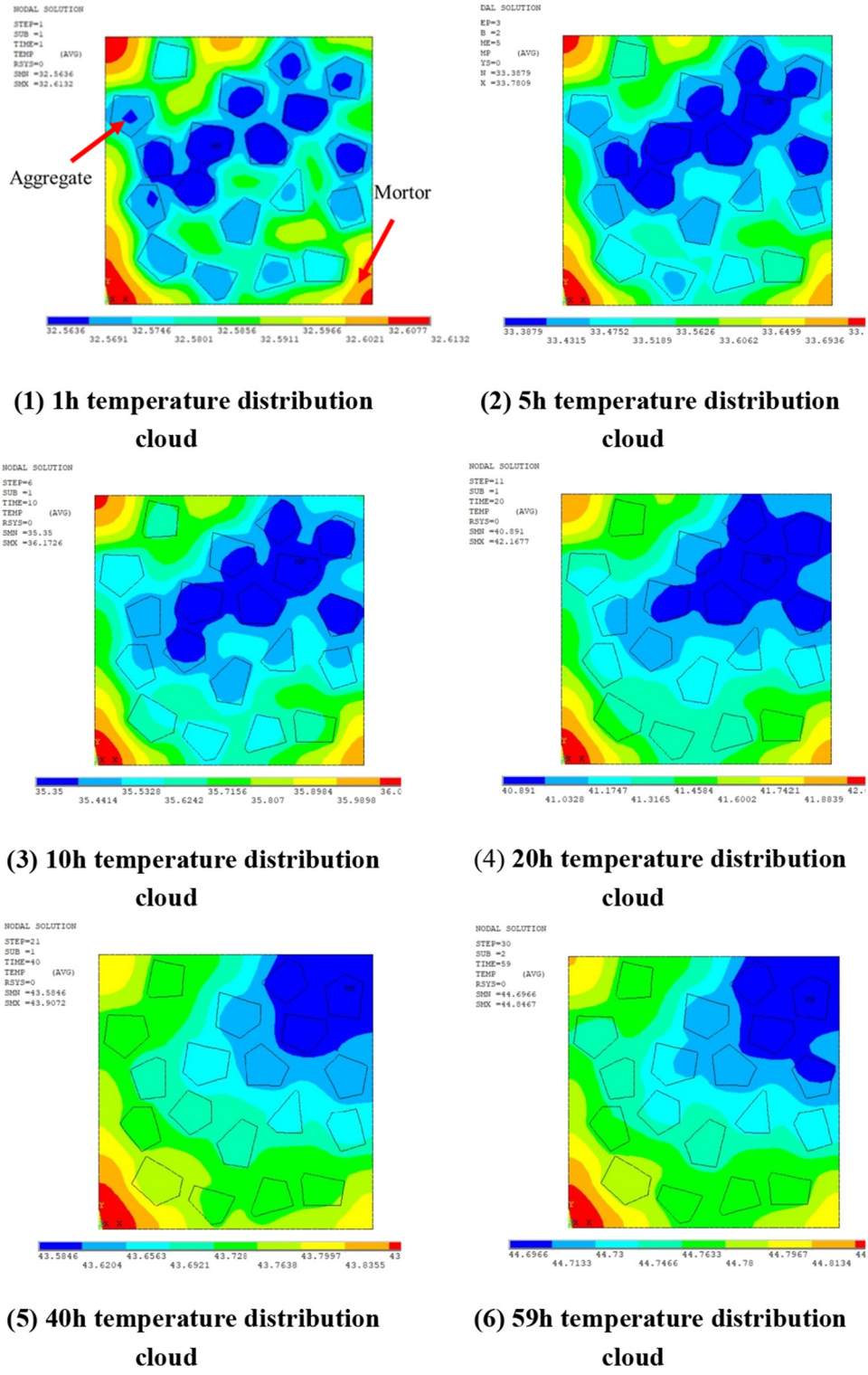

Figure 5: Cloud picture of temperature distribution changes.

is larger, which is due to the different material properties of mortar and aggregate, while the temperature distribution of the macroscopic model is relatively moderate, and the macroscopic model considers the cemented gravel as a homogeneous material and pays more attention to the study on the effect of the exotherm of the hydration of the cemented gravel and heat dissipation of the surface of the cemented gravel in contact with the air on the

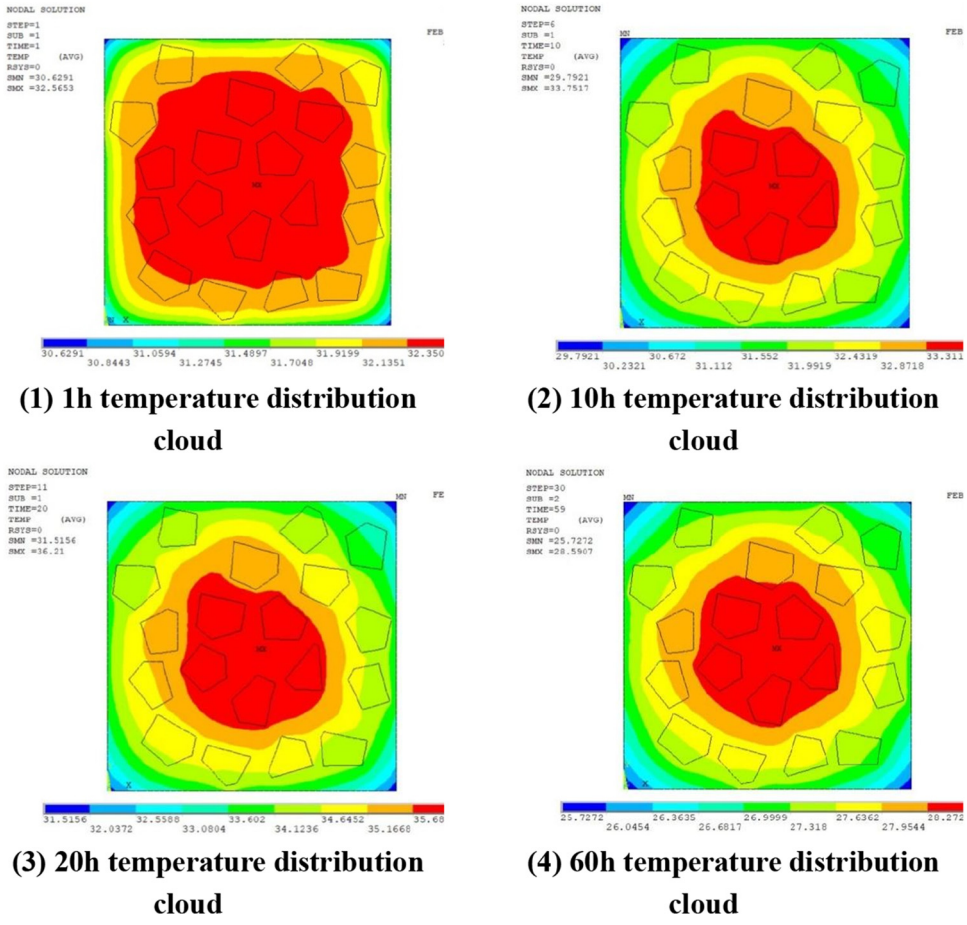

Figure 6: Cloud picture of temperature distribution changes.

distribution of the temperature field of cemented gravel. It focuses more on the effects of exothermic hydration of cemented gravel and heat dissipation from the surface of cemented gravel in contact with air on the distribution of the temperature field of cemented gravel.

3.3 Analysis of stress results

Based on the temperature field results, stress field calculations are performed as shown in Figures 3–7, 3–8, 3–9 and 3–10.

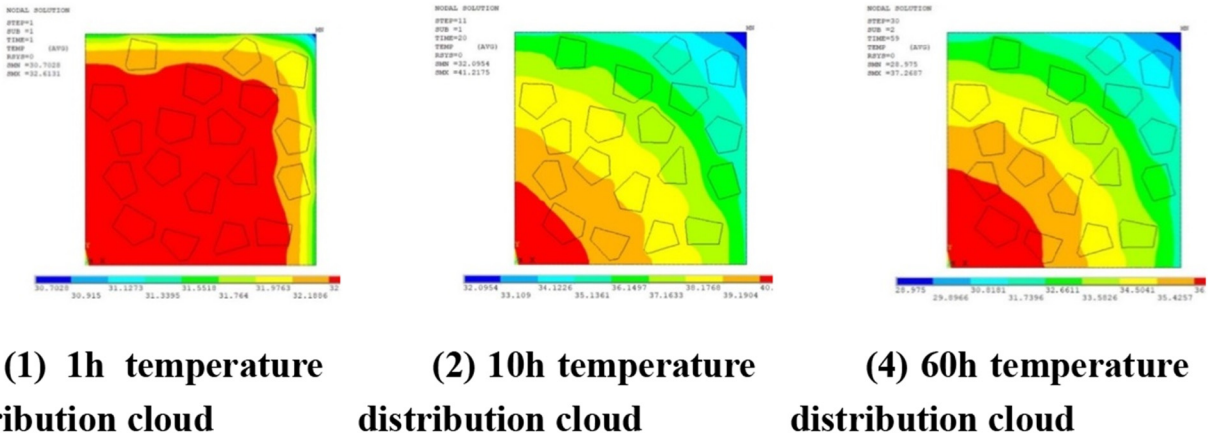

Figure 7: Cloud picture of temperature distribution changes.

3.3.1 Working condition 1

Observing the change of the first principal stress at each moment in Figure 9, it can be seen that the first principal stress of the simulated specimen decreases with time, in which the maximum value of the first principal stress at 1 h is about 0.157 MPa, and the tensile strength at early age is lower, and there is a risk of cracking. The other specimen tensile stress is mainly concentrated in the intersection surface of mortar and aggregate, which is due to the heat released by mortar hydration to the aggregate; there is a temperature difference between the two, but also due to the different moduli of elasticity of the two.

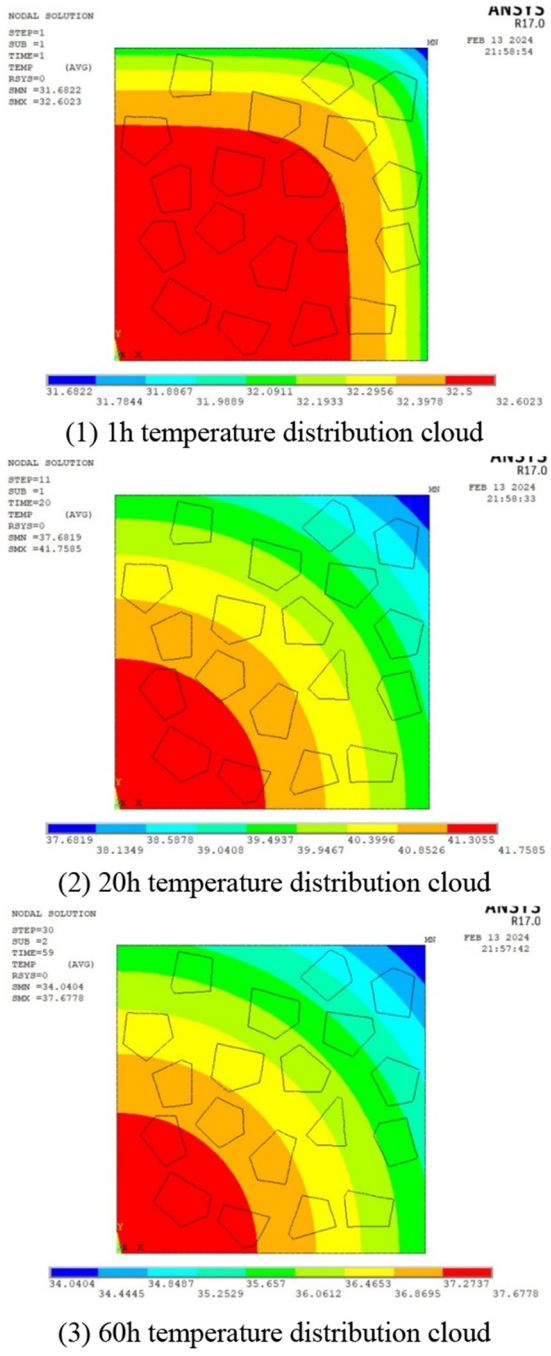

Figure 8: Cloud picture of temperature distribution changes.

3.3.2 Working condition 2

Comparing the first principal stress of condition 2 and condition 1 in Figure 10, it is found that the maximum first principal stress of condition 2 is greater than that of condition 1 at the same time. This is due to the heat dissipation around the CSG in condition 2, the temperature changes rapidly, the temperature difference is large, and the stress is large.

3.3.3 Working condition 3

Observing the simulation specimen's first principal stress distribution at each moment in Figure 11, it can be seen that 1 h hydration at the beginning of the adiabatic surface causes the temperature to gradually increase and the temperature change is faster, resulting in a larger first principal stress. The maximum first principal stress is about 0.215 MPa. It can also be seen that 60 h hydration exotherm is basically over, the simulation specimen temperature gradually tends to the ambient temperature, and the temperature difference change is small. The maximum first principal stress is about 0.0155 MPa.

3.3.4 Working condition 4

As shown in Figure 12, compared with working condition 4 and working condition 3, the first principal stress of working condition 4 is small, mainly distributed at the boundary of the heat dissipation surface, while the maximum first principal stress in working condition 3 is concentrated on the intersection surface of mortar and aggregate. The reason is that in working condition 4, the CSG are regarded as homogeneous materials, and the heat is transferred to the heat dissipation surface. The gradient here is large, and the stress is large. However, in working condition 3, the mortar is exothermic, and the aggregate is not exothermic. There is a temperature difference between the two. Due to the random distribution of aggregate, the stress distribution shows the characteristics of concentration and dispersion. In addition, as the weak link of stress, the interface is easier to crack, which is the focus of future attention.

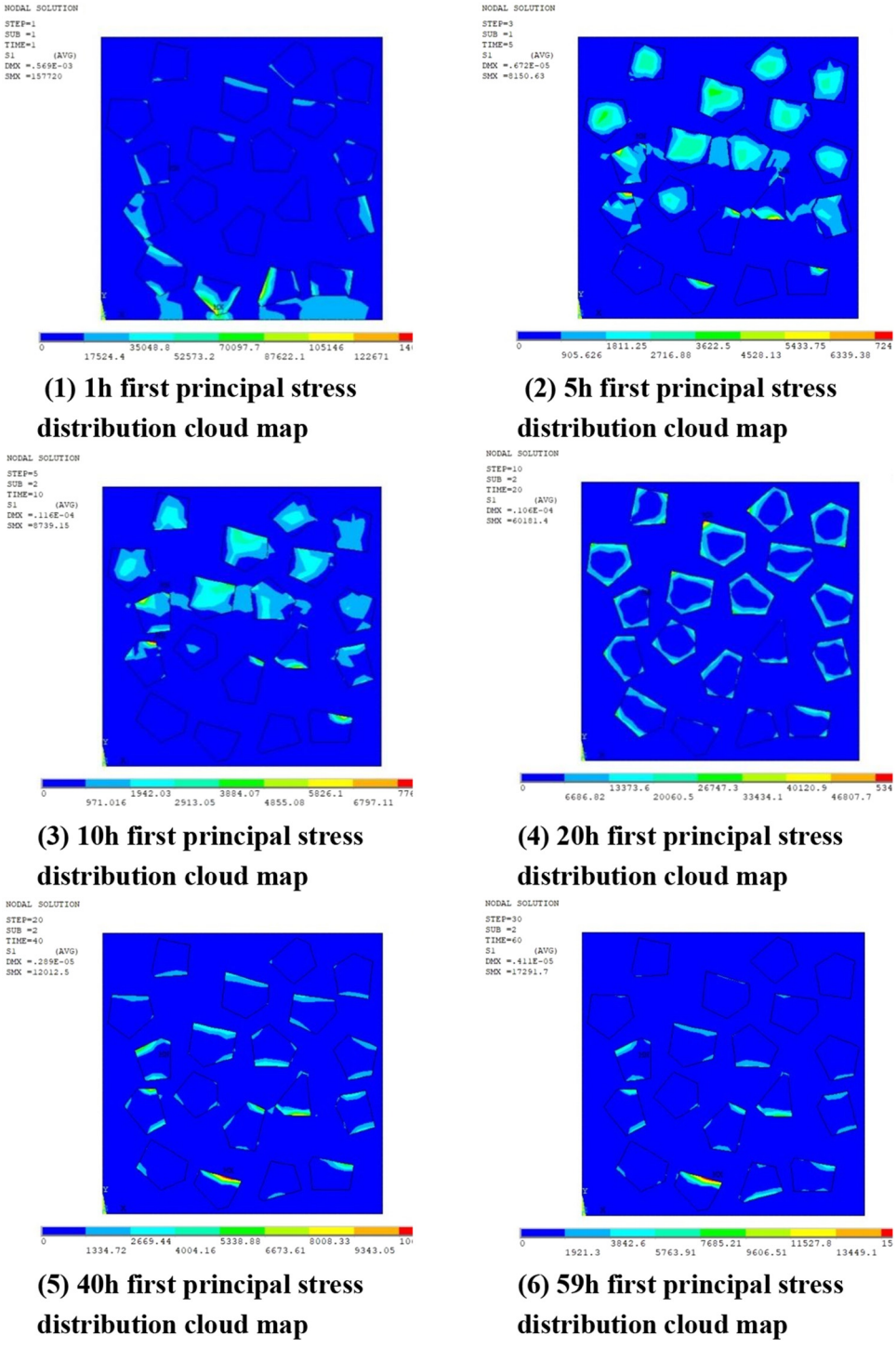

Figure 9: Cloud picture of the first principal stress change.

4 Conclusion

In this article, according to the characteristics of CSG aggregate, the random polygon aggregate model is established by using ANSYS finite-element software. According to the test results of CSG, the meso parameters are inverted, and the temperature stress variation law of CSG considering meso parameters and not considering meso parameters

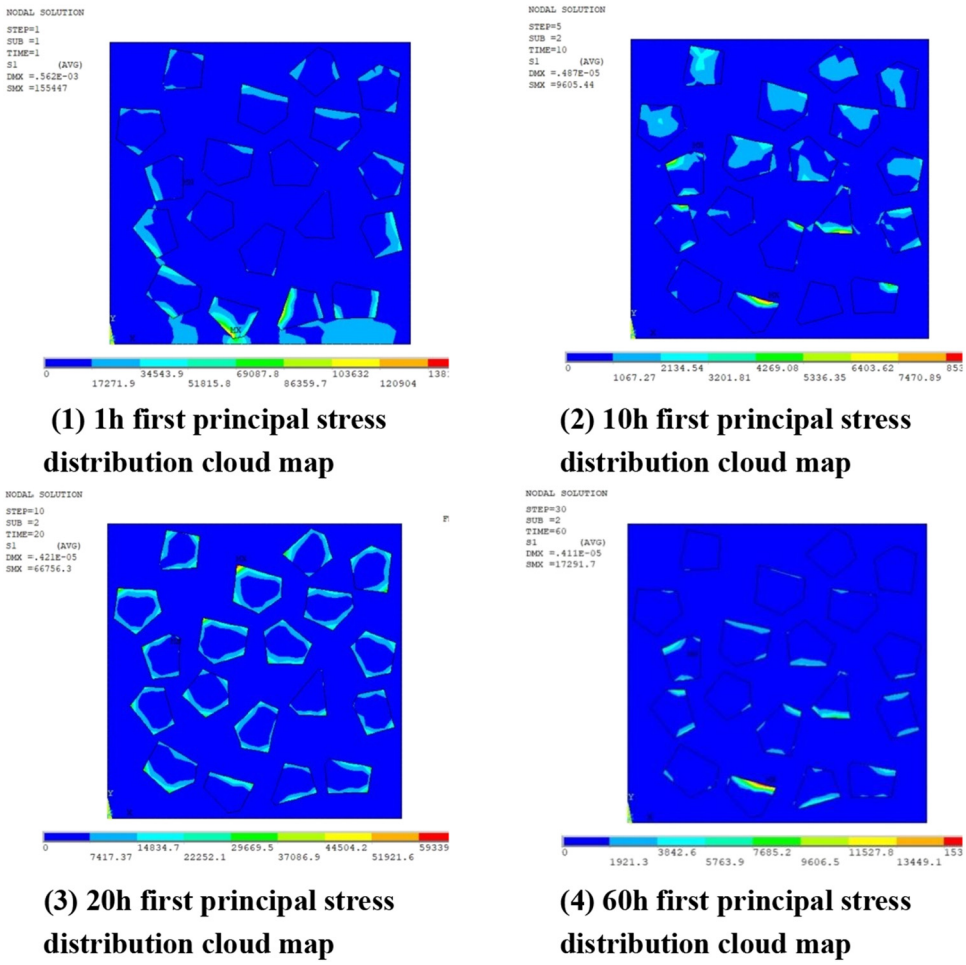

Figure 10: Cloud picture of the first principal stress change.

under different working conditions is studied. The following conclusions are obtained:

(1) Under different boundary conditions, the temperature field distribution of CSG is different. In the case of considering the meso-component, the temperature of the CSG specimen in the adiabatic state gradually increases with time. There is a certain temperature difference between the mortar and the aggregate inside the specimen, and it gradually tends to be isothermal with time. The temperature of the CSG specimen in the heat dissipation state increases first and then decreases with time and gradually maintains an isothermal state with the ambient temperature. The temperature gradient changes rapidly. The internal temperature difference of the specimen is large at the heat dissipation boundary, and the temperature difference between the mortar and the aggregate is not obvious.

(2) The magnitude of the first principal stress of CSG changes with the change of temperature difference. The greater the temperature difference, the greater the first principal stress. If the CSG does not consider the microscopic components, the first principal stress increases first and then decreases with time under the heat dissipation state, and the larger stress is concentrated at the boundary heat dissipation. If the meso-components are considered, in the adiabatic state, the first principal stress increases with time in a wave-like manner, and the maximum stress is mainly concentrated on the intersection surface of mortar and aggregate. However, due to the random distribution of aggregate, the maximum stress is

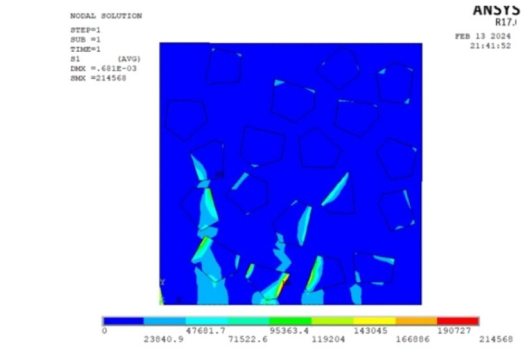

(1) 1h first principal stress distribution cloud map

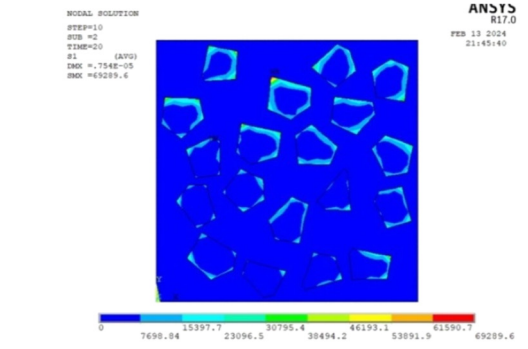

(2) 20h first principal stress distribution cloud map

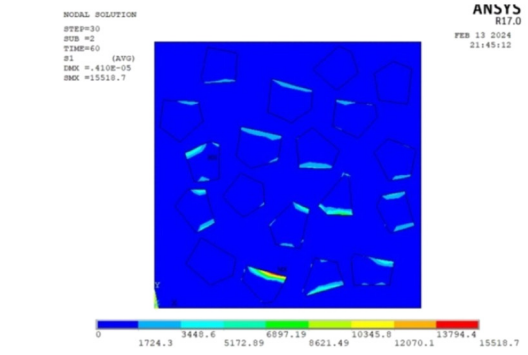

(3) 60h first principal stress distribution cloud map

Figure 11: Cloud picture of the first principal stress change.

dispersed. In the heat dissipation state, the first principal stress increases with time and then decreases. The stress distribution is uneven, and the maximum stress is concentrated on the intersection surface of mortar and aggregate.

In summary, considering the finite-element analysis results of meso-components, stress concentration is more likely to occur at the interface, and the risk of cracking is increased due to the low strength of early-age CSG, which provides a theoretical basis for crack control in engineering practice.

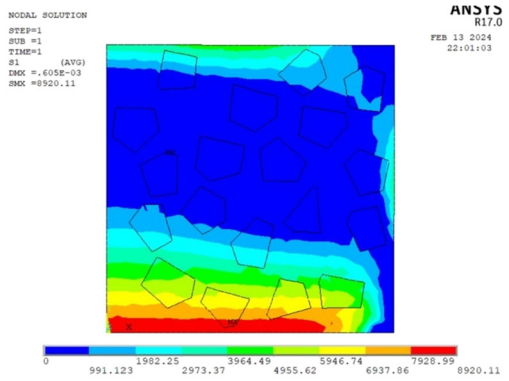

(1) 1h first principal stress distribution cloud map

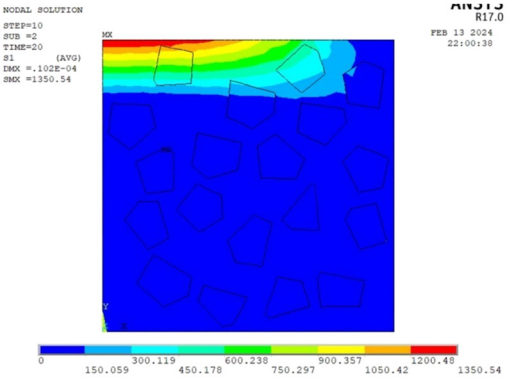

(2) 20h first principal stress distribution cloud map

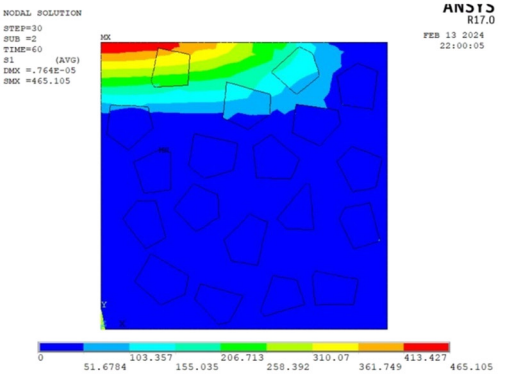

(3) 60h first principal stress distribution cloud map

Figure 12: Cloud picture of the first principal stress change.

Funding information: This study was funded by the third section of the project scientific research service project (HNYJJH/JS/FWKY-2021003) of the Yangtze River to Huaihe River Project (Henan section).

Author contributions: All authors have accepted responsibility for the entire content of this manuscript and consented to its submission to the journal, reviewed all the results, and approved the final version of the manuscript.

L.G. designed the study and conducted the experiments; T.L. developed the random aggregate model and performed numerical simulations; L.Z. supervised the research, secured funding, and revised the manuscript.

Conflict of interest: Authors state no conflict of interest.

Data availability statement: All data, models, and code generated or used during the study appear in the published article.

References

[1] Mehta PK. Greening of the concrete industry for sustainable development. Concr Int. 2002 Jul;24(7):23–8.

[2] Karimi S, Farshbaf Aghajani H. The strength and microstructure of cemented sand-gravel (CSG) mixture containing fine-grained particles. Int J Geo-Engineering. 2023 Feb;14(1):5.

[3] Amini Y, Hamidi A, Asghari E. Shear strength–dilation characteristics of cemented sand–gravel mixtures. Int J Geotech Eng. 2014 Oct;8(4):406–13.

[4] Londe P. The faced symmetrical hardfill dam: A new concept for RCC. Water Power Dam Constr. 1992;19–24.

[5] Jia J, Michel L, Jin F, Zheng C. Cemented material dam (CMD)—An environmentally friendly new dam type. Engineering. 2016;2(4):220–35.

[6] Zhu BF. Temperature stress and temperature control of hydraulic concrete structures. Beijing: Water Conservancy and Electric Power Press; 1976. p. 127–31.

[7] Zhu BF. Expression for adiabatic temperature rise of concrete considering temperature effects. J Hydropower Gener. 2003;2:69–73.

[8] Wu P, Guo L, Luo G, Sun M. Freeze-Thaw simulation analysis of cemented sand and gravel dam during operation period based on damage theory. Water Resour Power. 2017;35(1):81–4.

[9] Liu Z, Tian Y, Wang M. Study on temperature stress of cemented sand and gravel dam. Shanxi Archit. 2018;44(30):212–3.

[10] Liu B, He Y, Peng Y. Simulation analysis of temperature field for hardfill dam. Yangtze River. 2008;39(14):92–5.

[11] Wu H, Peng Y, Yuan Y. Study on simplified construction temperature control measures for cemented sand and gravel dam. Water Resour Hydropower Eng. 2015;46(1):76–79+84.

[12] Xu B. Temperature-controlled freeze-thaw simulation of colluvial gravel dams. Master's thesis. Zhengzhou, China: North China University of Water Resources and Hydropower; 2022.

[13] Fu Y. Study on seepage characteristics and temperature control simulation of cemented sand and gravel dam. Master's thesis. Zhengzhou, China: North China University of Water Resources and Electric Power; 2021.

[14] Zhao X, He Y. Influence of seepage field on temperature field in cemented sand and gravel dam. Eng J Wuhan Univ (Eng Sci Ed). 2020;53(4):283–92.

[15] Cai X, Jiang M, Guo X, Chen J, Zhao Q. Experimental study on the creep behaviour of cemented sand and gravel (CSG) and temperature stress prediction of CSG dam under seasonal temperature change. Adv Civ Eng. 2020;2020(1):8289520.

[16] Chen S, Zheng Y. Study on the evolutionary model and structural simulation of the freeze–thaw damage of cemented sand and gravel (CSG). J Inst Eng (India): Ser A. 2018 Dec;99:699–704.

[17] Jiang M, Cai X, Guo X, Liu Q, Zhang T. Adiabatic temperature rise test of cemented sand and gravel (CSG) and its application to temperature stress prediction of CSG dam. Adv Mater Sci Eng. 2020;2020(1):3898391.

[18] Huang Y, Yang Z, Ren W, Liu G, Zhang C. 3D meso-scale fracture modelling and validation of concrete based on in-situ X-ray Computed Tomography images using damage plasticity model. Int J Solids Struct. 2015 Aug;67:340–52.

[19] Huang YJ, Guo FQ, Zhang H, Yang ZJ. An efficient computational framework for generating realistic 3D mesoscale concrete models using micro X-ray computed tomography images and dynamic physics engine. Cem Concr Compos. 2022 Feb;126:104347.

[20] Feng W, Jia J, Ma F. Study on mix proportion design parameters of cemented sand and gravel material. Water Resour Hydropower Eng. 2013;44(2):55–8. doi: 10.13928/j.cnki.wrahe.2013.02.022.

[21] Guo Q, Pei L, Zhou Z, Chen J, Yao F. Response surface and genetic method of deformation back analysis for high core rockfill dams. Computers Geotech. 2016 Apr;74:132–40.

[22] Wang J, Wu L, Mi K, Wen Q. Numerical simulation of two-dimensional random polygonal aggregate model for three-graded concrete. Yangtze River. 2015;46(11):71–5.

[23] Guo L, Duan Y, Sun M. Adiabatic temperature rise model and its application for cemented sand and gravel material. Yellow River. 2016;38(7):89–91.

[24] Wang Y, Sun X. Research on adiabatic temperature rise model of concrete. J Highw Transport Res Dev (Appl Technol Ed). 2017;13(10):31–3.

[25] Sun J, Ge B, Li S, Zhao Y, Sun F. Research on modification of concrete adiabatic temperature rise model. N Build Mater. 2023;50(6):17–21.

[26] Huang H, Li P, Huo W, Zhang X. Study on macro- and meso-parameters and failure modes of cemented sand and gravel materials. J North China Univ Water Resour Hydropower (Natural Science Edition). 2020;(04):27–38. doi: 10.19760/j.ncwu.zk.20200046.

[27] Li S. Research on the influence of aggregate characteristics on the properties of cemented sand and gravel and optimization. Master's thesis. Zhengzhou, China: North China University of Water Resources and Hydropower; 2022.

[28] Lu Q, Zhu X, Hui Y Influence of thermal expansion coefficient on thermal stress in concrete. Water Resour Power. 2010;28(8):106–7+170.